Scientia Iranica B (2023) 30(3), 1039–1048

Sharif University of Technology
Scientia Iranica
Transactions B: Mechanical Engineering
http://scientiairanica.sharif.edu

Research Note

Numerical simulation of melting heat transfer towards the stagnation point region over a permeable shrinking surface

K. Zheng[a], S.I. Shah[b], M. Naveed Khan[c,*], E. Tag-eldin[d], M. Yasir[c], and A.M. Galal[e,f,*]

a. *College of Water Conservancy and Ecological Engineering, Nanchang Institute of Technology, Nanchang 330099, China.*
b. *Department of Sciences and Humanities, National University of Computer and Emerging Sciences (FAST), A. K. Brohi Road H-11/4 Islamabad, Pakistan.*
c. *Department of Mathematics, Quaid-i-Azam University, Islamabad, Pakistan.*
d. *Faculty of Engineering and Technology, Future University in Egypt New Cairo 11835, Egypt.*
e. *Department of Mechanical Engineering, College of Engineering, Prince Sattam Bin Abdulaziz University, Wadi Addawaser 11991, Saudi Arabia.*
f. *Department of Production Engineering and Mechanical Design, Faculty of Engineering, Mansoura University, P.O 35516, Mansoura, Egypt.*

Received 13 February 2022; received in revised form 22 May 2022; accepted 21 November 2022

KEYWORDS
Numerical solution;
Melting heat transfer;
Thermal radiation;
Ohmic heating;
Viscous dissipation.

Abstract. The aim of deploying hybrid nanofluids is to optimize the thermal transport characteristics of the model under study. Hybrid nanofluids incorporate composite nanoparticles that enhance thermal conductivity. Here, Silver (Ag) and Graphene oxide (Go) are used as nanoparticles with kerosene oil as the base fluid. The impacts of Ohmic heating, viscous dissipation, and thermal radiation are considered in order to model the problem of steady flow over a stretching/shrinking geometry. The model equations are tackled by a built-in scheme, bvp4c, in MATLAB. Moreover, there are dual solutions for a given range of pertinent parameters. The impact of the melting heat transfer parameter on the coefficient of skin friction and Nusselt number for both hybrid nanofluid and nanoparticles is considered. A comparison is established between our results and the pre-existing results, which are in good agreement. It is noted that the values of the coefficient of friction drag for the upper branch are reduced for a particular range of shrinking parameter values, while the opposite trend is observed for the lower branch. The magnetic force reduces the flow field and energy distribution for the stable branch while increasing them for the lower branch.

1. Introduction

Recent discovery of hybrid nanocomposites has piqued curiosity about their possible applications in a variety of fields. Hybrid nanofluids combine metallic, polymeric, or non-metallic nanoparticles with a base fluid to boost heat transmission. They are known for their great electrical and thermal conductivity. Their exceptional dynamic strengths and specific heat result from their nanostructure and particle bonds. These features are expected to aid various fields of industry and technology, including telecommunications, ophthalmology, thermoplastic elastomers, biotechnology, etc. Many research groups were motivated by Iijima's

*. *Corresponding authors.*
E-mail addresses: mnkhan@math.qau.edu.pk (M. Naveed Khan); ahm.mohamed@psau.edu.sa (A.M. Galal)

doi: 10.24200/sci.2022.59956.6518

discovery of carbon nanotubes in 1991 [1]. Huang et al. [2] studied the pressure drop and energy transport enhancement properties of hybrid nanofluid. By taking multiple diameters of water confined in single-walled carbon nanotubes, Liu et al. [3] investigated the flow transport and its structural properties. Madhesh and Kalaiselvam [4] experimentally noted the impact of forced convection on hybrid nanofluids through heat exchangers. Toghraie et al. [5] conducted experimental verification of nanoparticle concentration on energy enhancement for ZnO-TiO_2/EG. The hybrid nanofluid model with free convection within porous media was presented by Tlili et al. [6] They applied Finite Element Method (FEM) and Gauss-Seidel method to obtain the desired outcomes. Yang et al. [7] conducted thermal transport investigation for Casson nanofluid flow. Tang et al. [8] made a comparison of interfacial properties on crude oil-water with rheological attributes of polymeric nanofluids. Further recent studies related to hybrid nanofluid are presented in [9–16].

Melting heat transfer is a complicated and significant field of thermo-physics that is linked to phase-transition issues in production such as electromagnetic crucible systems, metallic processing, glass treatment, polymer synthesis, and laser ablation. In thermally driven flows, melting heat transfer simulation is complicated because the fluid dynamics must be combined with a moving interface. Such issues are commonly referred to as the "Stefan shifting boundary" problem. The melting process and heat transfer rate are the two most important elements to consider when evaluating the melting heat transfer process. To address melting heat transfer issues effectively and precisely as moving boundary problems, strong computational techniques are necessary. An alternative approach is to model the melting effect as a boundary condition, which avoids the need to explicitly simulate the moving interface. This method works with boundary layer flow models as well, but is less accurate. Roberts [17] first reported the melting behavior of an ice slab in a hot air stream. Yacob et al. [18] scrutinized the heat transfer in a micropolar fluid boundary layer stagnation point flow across a stretching/contracting sheet with a melting effect. Bachok et al. [19] explored the characteristics of melting heat transport in the viscous fluid flow toward a stretching surface. Hayat et al. [20] scrutinized the flow of Maxwell fluid towards a stretched surface with a melting phenomenon. The melting process in a magnetized flow over a moving surface with heat radiation was explored by Das [21]. The related similar studies can be found in [22–28].

The objective of this study is to reveal the properties of melting heat transfer in the flow of hybrid nanofluid flow across a stretching/shrinking surface in the stagnation point region. Here, kerosene oil is assumed as the base fluid, while silver (Ag) and Graphene oxide (Go) are the nanoparticles. The results for various physical parameters are obtained and presented graphically and in tables. In addition, the limiting case comparison results are based on previously published data.

2. Formulation of the problem

We assume a boundary layer flow of hybrid nanofluid on a shrinking surface, with melting heat transfer. It is assumed that the external flow velocity is $u_e(x) = ax$, where the stretching/shrinking velocity is $u_w(x) = bx$. The coordinate system is selected such that the direction of the flow be along the $x - axis$ and the $y - axis$ be perpendicular to it. The magnetic force with strength B_o is imposed in a vertical direction. Moreover, nonlinear thermal radiation with Ohmic heating and viscous dissipation is taken into account in order to describe the thermal transport of a hybrid nanofluid. The melting surface temperature is assumed to be T_m, whereas the free-stream temperature is T_∞, where $T_\infty > T_m$. The flow structure of our considered problem is depicted in Figure 1. Using the assumption above, the flow problem is designed as follows:

$$\frac{\partial u}{\partial x} + \frac{\partial v}{\partial y} = 0, \quad (1)$$

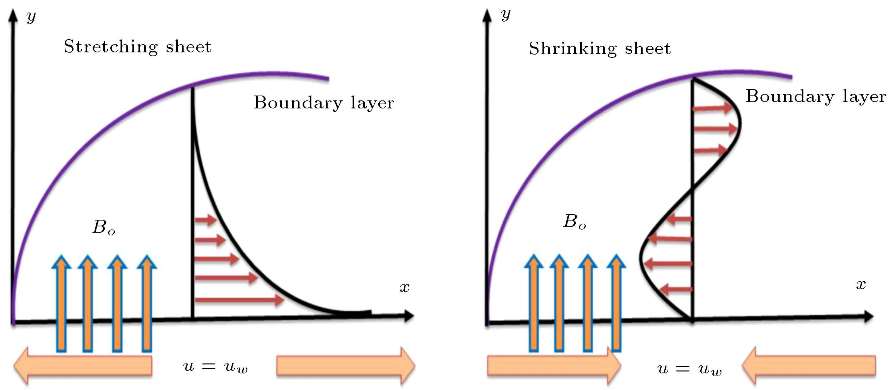

Figure 1. Geometry of the problem.

$$\left.\begin{array}{c} u = u_w,\, T = T_m,\, k_{hnf}\left(\frac{\partial T}{\partial y}\right) = \rho_{hnf}\left\{L + c_{s(T_m - T_0)}\right\} v\,(x,\, y) \text{ at } \ y = 0 \\ u \to u_e \ \text{ and } \ T \to T_\infty, \ \text{ as } \ y \to \infty \end{array}\right\}. \tag{4}$$

Box I

$$u\frac{\partial u}{\partial x} + v\frac{\partial u}{\partial y} = u_e\frac{du_e}{dx} + \frac{\mu_{hnf}}{\rho_{hnf}}\frac{\partial^2 u}{\partial y^2} + \frac{\sigma_{hnf}B_o^2}{\rho_{hnf}}\left(u_e - u\right), \tag{2}$$

$$u\frac{\partial T}{\partial x} + v\frac{\partial T}{\partial y} = \frac{1}{(\rho c_p)_{hnf}}\left\{k_{hnf} + \frac{16\sigma^* T^3}{3k^*}\right\}\frac{\partial^2 T}{\partial y^2} + \frac{\mu_{hnf}}{(\rho c_p)_{hnf}}\left(\frac{\partial u}{\partial y}\right)^2 + \frac{\sigma_{hnf}B_o^2(u - u_e)^2}{(\rho c_p)_{hnf}}. \tag{3}$$

The boundary conditions is obtained by Eq. (4) as shown in Box I. Letting:

$$u = axf'(\eta)\,, \qquad v = -\sqrt{a\nu_f}\,f(\eta)\,,$$
$$\theta = \frac{T - T_m}{T_\infty - T_m}, \qquad \eta = \sqrt{\frac{a}{\nu_f}}\,y, \tag{5}$$

which satisfies Eq. (1) and converts the motion equation into the following:

$$\frac{1}{\rho_{hnf}/\rho_f}\left(\frac{\mu_{hnf}}{\mu_f}f'''\right) + ff'' - f'^2 + \frac{\sigma_{hnf}/\sigma_f}{\rho_{hnf}/\rho_f}M\left(1 - f'\right) + 1 = 0, \tag{6}$$

Eq. (7) is shown in Box II. With the boundary condition Eq. (8) is obtained as shown in Box III. The involved physical parameters are defined as follows: $\chi = \left(\frac{b}{a}\right)$ is the stretching/shrinking parameter, $M = \left(\frac{\sigma B_o^2}{a\rho_f}\right)$ the magnetic field parameter, $m_e = \left(\frac{(c_p)_f(T_\infty - T_m)}{L + c_s(T_m - T_o)}\right)$ the melting heat transfer parameter, $Pr = \left(\frac{\nu_f (c_p)_f}{k_f}\right)$ the Prandtl number, $R_d = \left(\frac{4\sigma^* T_\infty^3}{k_f k^*}\right)$ thermal radiation, $\theta_w = \left(\frac{T_m}{T_\infty}\right) > 1$ the temperature ratio parameter, and $Ec = \left(\frac{u_e^2}{(c_p)_f(T_\infty - T_m)}\right)$ the Eckert number.

3. Physical quantities

The expressions for physical quantities are expressed as follows:

$$C_f = \frac{\tau_w}{\rho_f u_e^2}, \quad \text{and} \quad Nu = \frac{xq_w}{k_f\left(T_\infty - T_m\right)}, \tag{9}$$

where τ_w and q_w denote the surface heat and mass fluxes that are defined as:

$$\tau_w = \mu_{hnf}\left(\frac{\partial u}{\partial y}\right)\bigg|_{y=0} \quad \text{and}$$
$$q_w = -\left(k_{hnf} + \frac{16\sigma^*}{3k^*}T^3\right)\left(\frac{\partial T}{\partial y}\right)\bigg|_{y=0}. \tag{10}$$

The dimensionless form of Eq. (10) is:

$$Re^{\frac{1}{2}}C_f = f''(0), \qquad \text{and} \qquad Re^{-\frac{1}{2}}Nu = -\left\{\frac{k_{hnf}}{k_f} + \frac{4}{3}R_d\left\{1 + (\theta_w - 1)\,\theta(0)\right\}^3\right\}\theta'(0), \tag{11}$$

in which $Re = \left(\frac{u_e x}{\nu}\right)$ denotes the local Reynolds number.

$$\left.\begin{array}{c} \frac{1}{Pr}\frac{1}{(\rho c_p)_{hnf}/(\rho c_p)_f}\left\{\left(\frac{k_{hnf}}{k_f} + \frac{4}{3}R_d\{1 + (\theta_w - 1)\,\theta\}^3\right)\theta'\right\}' + f\theta' \\ + \frac{Ec}{(\rho c_p)_{hnf}/(\rho c_p)_f}\left\{\frac{\mu_{hnf}}{\mu_f}f''^2 + \frac{\sigma_{hnf}}{\sigma_f}M(1 - f')^2\right\} = 0 \end{array}\right\}. \tag{7}$$

Box II

$$\left.\begin{array}{c} f' = \chi,\, \theta = 0,\, m_e\frac{k_{hnf}}{k_f}\theta' + Pr\frac{\rho_{hnf}}{\rho_f}f = 0 \ \text{ at } \ y = 0, \\ f' \to 1,\, \theta \to 1 \ \text{ as } \ \eta \to \infty \end{array}\right\}. \tag{8}$$

Box III

4. Results and discussion

With the help of the shooting method, the governing Eqs. (6) and (7) as well as the boundary condition (8) are numerically solved. The dimensionless fluid velocity and temperature distribution, as well as the skin friction coefficient and heat transfer rate, are depicted graphically in Figures 2 to 12 as a result of changing various physical parameters. Throughout the analyses, the numerical significance is assigned to grasp the physical purpose of the problem, $M = 0.1$, $m_e = 0.5$, $\chi = -0.2$, $R_d = 1.0$, $\theta_w = 1.1$, and $Ec = 0.1$. In particular, the numerical values of $Re^{\frac{1}{2}}C_f$ and $Re^{-\frac{1}{2}}N_u$ against the shrinking parameter χ with $M = (0.1, 0.3, 0.5)$ are depicted in Figure 2(a) and (b). From these illustrated upshots, we concluded that the necessary values changed from the left to the right when the magnetic parameter varied from 0.1 to 0.5, corresponding to $\chi_c = -2.8412$ and $\chi_c =$

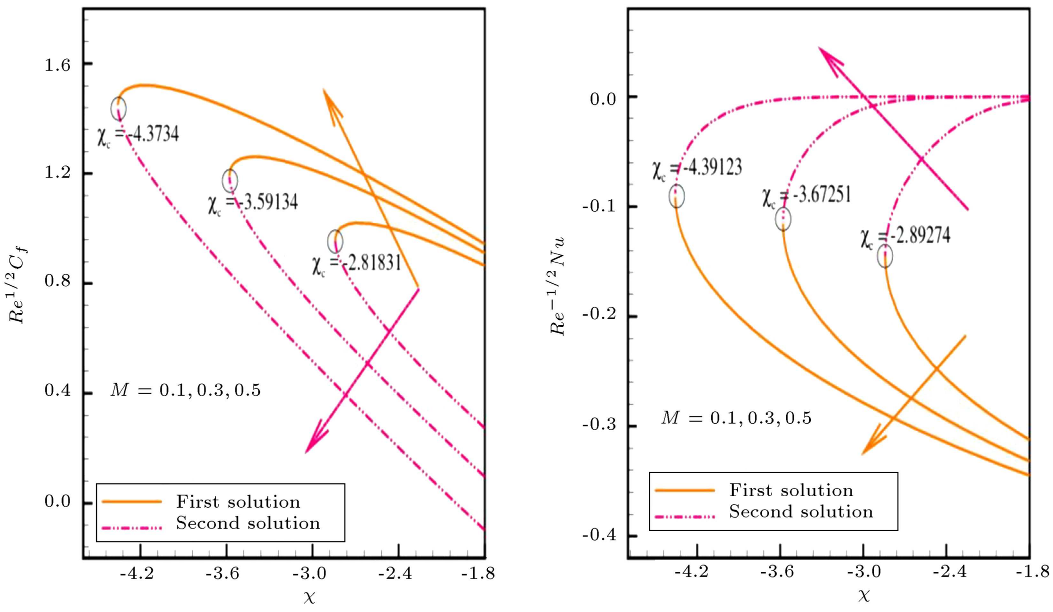

(a) (b)

Figure 2. Plot of M via $Re^{\frac{1}{2}}C_f$ and $Re^{-\frac{1}{2}}Nu_x$.

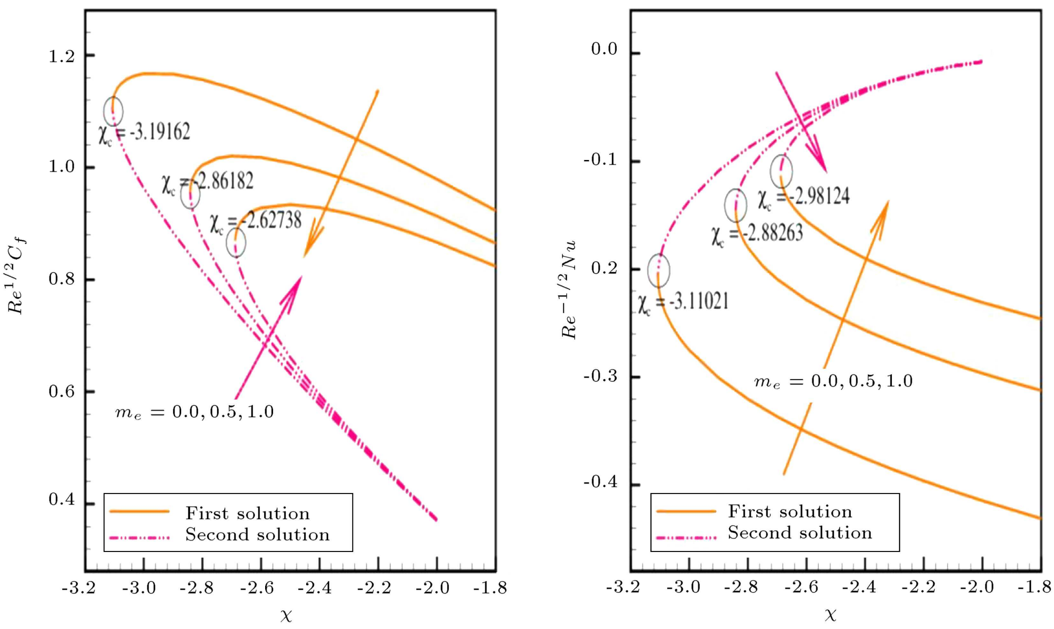

(a) (b)

Figure 3. Plot of m_e via $Re^{\frac{1}{2}}C_f$ and $Re^{-\frac{1}{2}}Nu_x$.

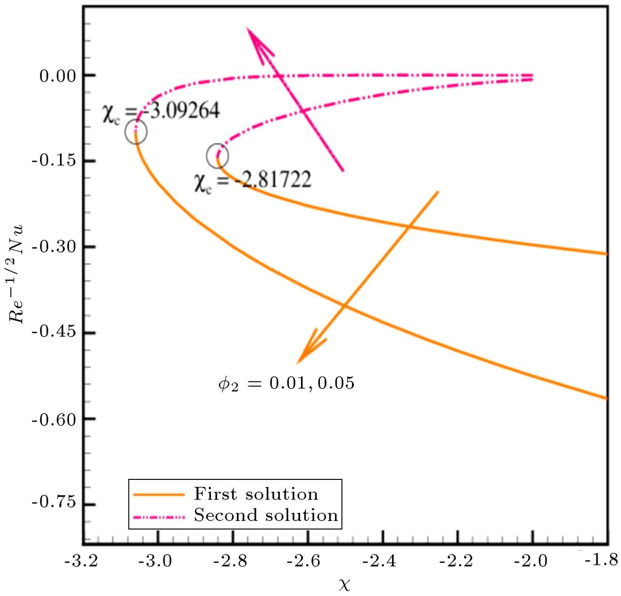

Figure 4. Plot of ϕ_2 via $Re^{-\frac{1}{2}}Nu_x$.

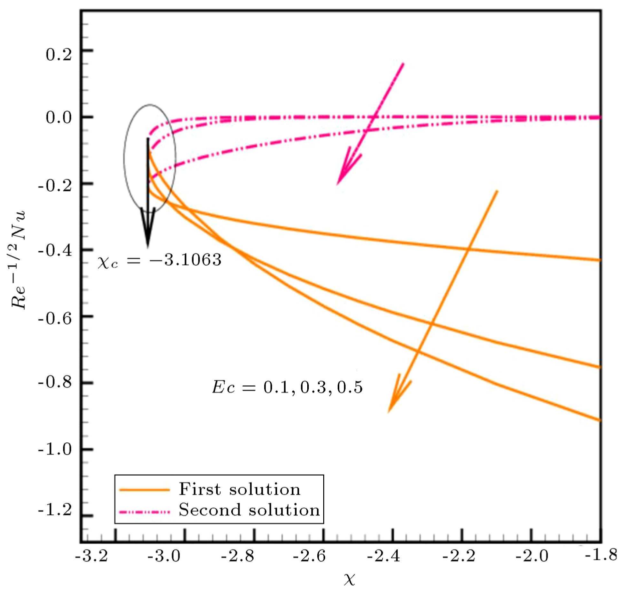

Figure 5. Plot of Ec via $Re^{-\frac{1}{2}}Nu_x$.

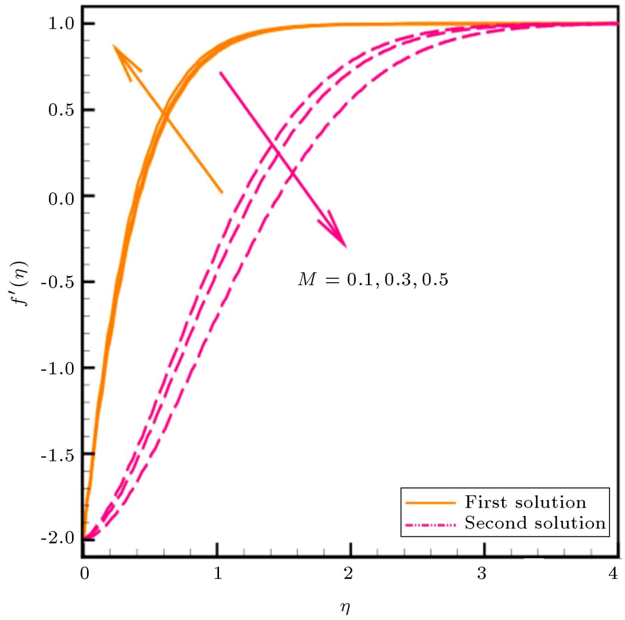

Figure 6. Plot of M via $f'(\eta)$.

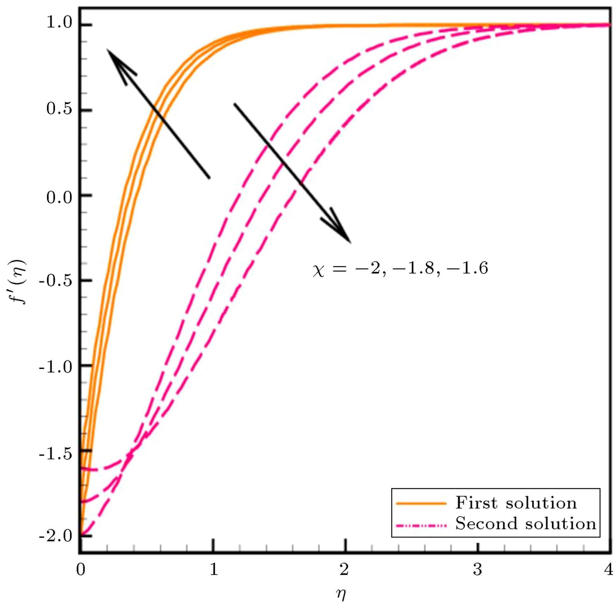

Figure 7. Plot of χ via $f'(\eta)$.

-4.3573. These Bifurcation values make it clear that both branches of the solutions exist in the range $\chi_c < \chi$, whereas no solution is found outside of turning points or when $\chi < \chi_c$; only one branch is discovered when $\chi = \chi_c$. Figure 3(a) and (b) shows the impact of m_e against the shrinking parameter χ on $Re_x^{1/2}C_{f_x}$ and $Re_x^{1/2}Nu_x$. These conclusions show that improving the melting parameter force reduces the skin friction coefficient and heat transfer rate (in an absolute sense). Figure 4 shows how the volume fractions of nanoparticles affect the heat transfer rate. Physically, due to an increase in the kinetic energy of the system, the heat transfer rate declines. This increase in kinetic energy improves the heat transfer rate in the upper branch solution. The consequence of the Eckert number Ec on $Re_x^{1/2}Nu_x$ is depicted in Figure 5. Here, it is noted that the suspense in a boundary layer separation is unaffected by boosting the Eckert number. Therefore, the dual solutions are exclusively valid up to the exact necessary value for all Ec's. The profiles $f'(\eta)$ for distinct values of Magnetic field parameter M and shrinking parameter χ are shown in Fiures 6 and 7, respectively. The increment in the values of these constraints improved the velocity of the fluid in the upper solution branch, while it declined in the lower solution branch. Figure 8 illustrates the impact of nanoparticle volume fraction on the

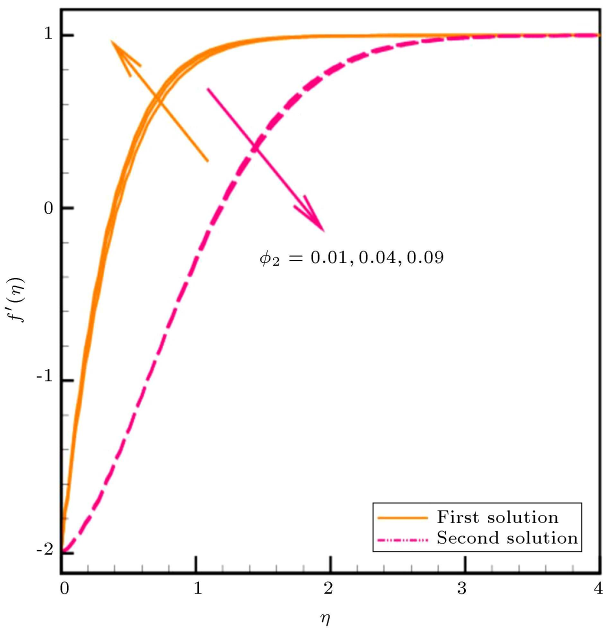

Figure 8. Plot of ϕ_2 via $f'(\eta)$.

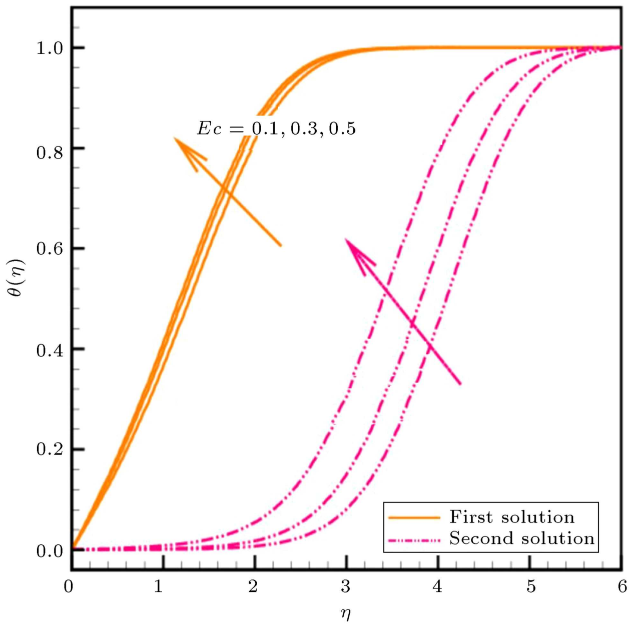

Figure 10. Plot of Ec via $\theta(\eta)$.

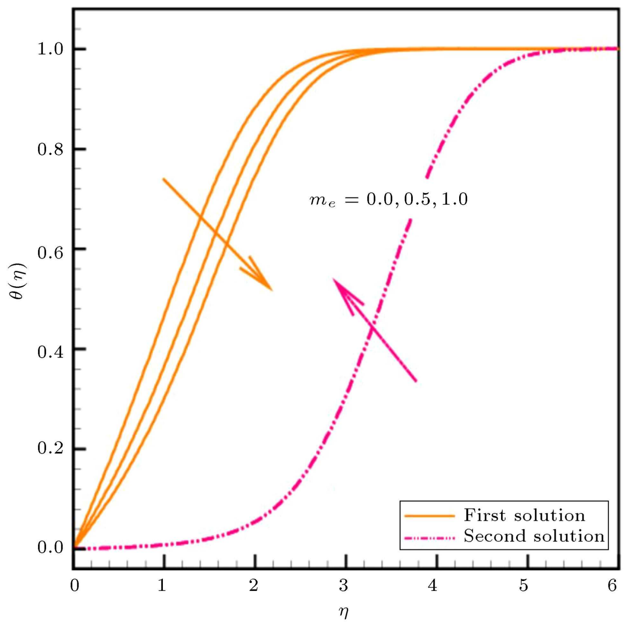

Figure 9. Plot of m_e via $\theta(\eta)$.

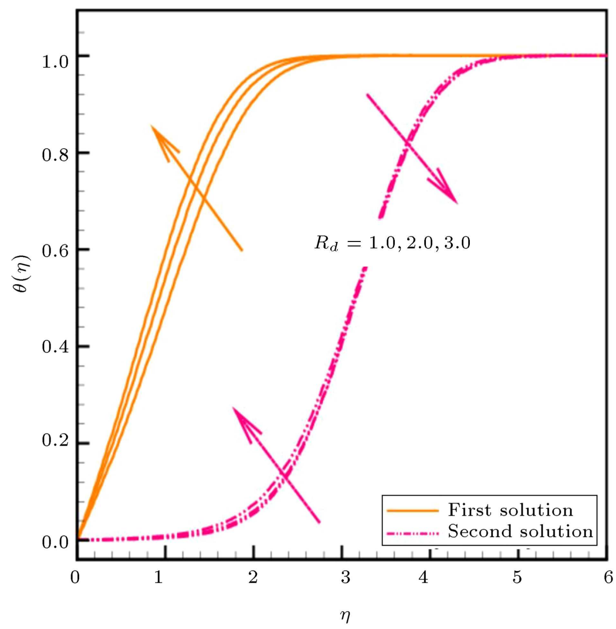

Figure 11. Plot of R_d via $\theta(\eta)$.

fluid velocity. Physically, the conduct is an outcome of intermolecular oscillations of nanoparticles, thus improving mass diffusion and reducing the flow field. Figure 9 shows how the temperature curves are affected by the melting parameter m_e. Further, it is noted that when the melting parameter increases, the first solution decays, whereas the second solution expands. According to Figure 10, the temperature distribution is elevated even at larger Eckert number Ec. Higher values of Ec physically retain more heat energy in the fluid. Therefore, the friction forces ultimately improve the temperature profile. In Figure 11, there has been an increasing trend in the thermal distribution for the radiation parameter R_d. The dominance of heat radiation over conduction is, therefore, indicated by higher values of R_d. As a result, rising values show that the system is absorbing more radiative heat energy, which raises the value of $\theta(\eta)$. Temperature distribution in the presence of melting heat increases in the case of the upper and lower branch solutions as the temperature ratio parameter θ_w increases in value, as shown in Figure 12.

Thermophysical properties of hybrid nanofluid and nanofluid are [29]:

Table 1. Thermo-physical properties [29].

Physical properties	c_p (J/kgK)	k (W/mK)	ρ (kg/m^3)	σ (S/m^1)
Ag	235	429	10500	63×10^{-6}
Go	717	5000	1800	6.30×10^{7}
Kerosene oil	2090	0.145	783	21×10^{-6}

Table 2. The numerical values of $f''(0)$ for shrinking parameter χ when $m_e = 0$.

	Bachok et al. [19]		Wang [30]		Present study	
χ	F.S.	S.S.	F.S.	S.S.	F.S.	S.S.
–1.0	1.3288170	0	1.32882	0	1.328873	0
–1.1	1.1866805	0.0492290	–	–	1.186642	0.049924
–1.15	1.0822315	0.1167022	1.08223	0.116702	1.082431	0.116863
–1.2	0.9324739	0.2336497	–	–	0.932743	0.235432

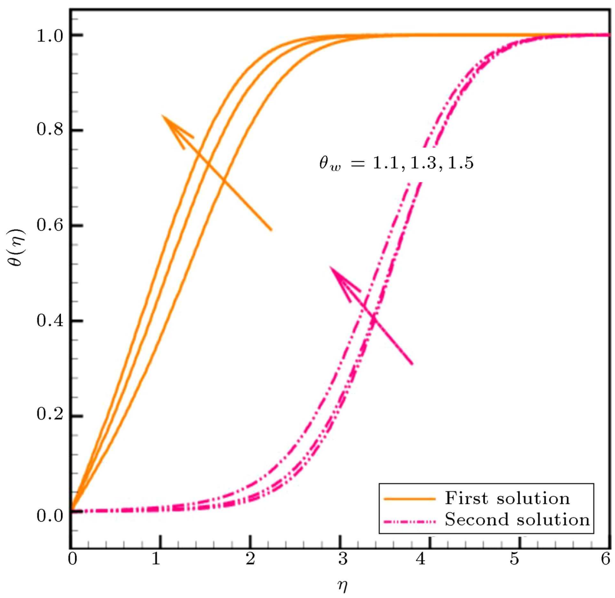

Figure 12. Plot of θ_w via $\theta(\eta)$.

$$\rho_{hnf} = (1-\phi_2)\left((1-\phi_1)\rho_f + \phi_1\rho_{m_1}\right) + \phi_2\rho_{m_2},$$

$$\left(\rho c_p\right)_{hnf} = (1-\phi_2)\left((1-\phi_1)(\rho c_p)_f + (\rho c_p)_{m_1}\phi_1\right) + \phi_2(\rho c_p)_{m_2},$$

$$\frac{k_{hnf}}{k_f} = \frac{k_{m_2}+2k_{nf}-2\left(k_{nf}-k_{m_2}\right)\phi_2}{k_{m_2}+2k_{nf}+\left(k_{nf}-k_{m_2}\right)\phi_2},$$

where:

$$\frac{k_{nf}}{k_f} = \frac{k_{m_1}+2k_f-2\left(k_f-k_{m_1}\right)\phi_1}{k_{m_1}+2k_f+\left(k_f-k_{m_1}\right)\phi_1},$$

$$\mu_{hnf} = \frac{\mu_f}{(1-\phi_1)^{2.5}(1-\phi_2)^{2.5}},$$

$$\frac{\sigma_{hnf}}{\sigma_{nf}} = \frac{\sigma_{m_2}+2\sigma_{nf}-2\left(\sigma_{nf}-\sigma_{m_2}\right)\phi_2}{\sigma_{m_2}+2\sigma_{nf}+\left(\sigma_{nf}-\sigma_{m_2}\right)\phi_2}.$$

and:

$$\rho_{nf} = (1-\phi_1)\rho_f + \phi_1\rho_{m_1},$$

$$\left(\rho c_p\right)_{nf} = (1-\phi_1)\left(\rho c_p\right)_f + \phi_1\left(\rho c_p\right)_{m_1},$$

$$\frac{k_{nf}}{k_f} = \frac{k_{m_1}+2k_f-2\left(k_f-k_{m_1}\right)\phi_1}{k_{m_1}+2k_f+\left(k_f-k_{m_1}\right)\phi_1}$$

$$\mu_{nf} = \frac{\mu_f}{(1-\varphi_1)^{2.5}}, \qquad \frac{\sigma_{nf}}{\sigma_f} = \frac{\sigma_{m_1}+2\sigma_f-2\left(\sigma_f-\sigma_{m_1}\right)\phi_1}{\sigma_{m_1}+2\sigma_f+\left(\sigma_f-\sigma_{m_1}\right)\phi_1}.$$

Table 1 shows the thermo-physical properties of the base fluid of nanoparticles.

5. Tabular comparison

A comparison of $f''(0)$ for the shrinking case ($\chi < 0$) is shown in Table 2, which demonstrates a positive correlation with past research.

6. Concluding remarks

This study investigated the stagnation point flow of a hybrid nanofluid over a permeable shrinking surface. Using similarity transformations, the boundary layer governing equations were converted into nonlinear ordinary differential equations, which were then solved in MATLAB using bvp4c. The impact of several dimensionless constraints on fluid velocity and temperature distribution was scrutinized. The numerical results of friction drag and heat transfer rates were discussed concerning various parameters. The key findings of the study are as follows:

- An increase in the melting parameter value sped up the separation of the boundary layer and reduced the velocity and temperature profiles marginally;
- In the presence of magnetic parameter, the fluid velocity was reduced due to the produced Lorentz force;

- Larger radiative and temperature ratio parameter caused a significant increase in the thermal state and related boundary layer thickness;
- For the thermal radiation parameter, the temperature field of hybrid nano liquid was significantly enhanced;
- An increase in Eckert number and temperature ratio parameter enhanced the temperature of the fluid.

Acknowledgement

This study is supported via funding from Prince Sattam bin Abdulaziz University project number (PSAU/2023/R/1444).

Nomenclature

u, v	Velocity components [$\mathrm{ms^{-1}}$]
v_f	Kinematic viscosity [$\mathrm{m^2s^{-1}}$]
k_f	Thermal conductivity [$\mathrm{kgmK^{-1}s^{-3}}$]
ρ_f	Density [$\mathrm{kgm^{-3}}$]
μ_f	Dynamic viscosity [$\mathrm{kgm^{-1}s^{-1}}$]
α_f	Thermal diffusivity [$\mathrm{m^2s^-1}$]
$(c_p)_f$	Specific heat [$\mathrm{m^2K^{-1}}$]
ϕ_1	Ag volume fraction
ϕ_2	Go volume fraction
T	Fluid temperature [K]
T_∞	Ambient temperature [K]
M	Magnetic parameter
Pr	Prandtl number
χ	Stretching/shrinking parameter
m_e	Melting parameter
θ_w	Temperature ratio parameter
Ec	Eckert number
R_d	Thermal radiation

For hybrid nanofluid

k_{hnf}	Thermal conductivity [$\mathrm{kgmK^{-1}s^{-3}}$]
α_{hnf}	Thermal diffusivity [$\mathrm{m^2s^{-1}}$]
$(c_p)_{hnf}$	Specific heat [$\mathrm{m^2s^{-2}K^{-1}}$]
μ_{hnf}	Dynamic viscosity [$\mathrm{kgm^{-1}s^{-1}}$]
v_{hnf}	Kinematic viscosity [$\mathrm{m^2s^{-1}}$]
ρ_{hnf}	Density [$\mathrm{kgm^{-3}}$]

For nanofluid

k_{nf}	Thermal conductivity [$\mathrm{kgmK^{-1}s^{-3}}$]
α_{nf}	Thermal diffusivity [$\mathrm{m^2s^{-1}}$]
$(c_p)_{nf}$	Specific heat [$\mathrm{m^2s^{-2}K^{-1}}$]
μ_{nf}	Dynamic viscosity [$\mathrm{kgm^{-1}s^{-1}}$]
v_{nf}	Kinematic viscosity [$\mathrm{m^2s^{-1}}$]
ρ_{nf}	Density [$\mathrm{kgm^{-3}}$]

References

1. Iijima, S. "Helical microtubules of graphitic carbon", *Nature*, **354**(6348), pp. 56–58 (1991).
2. Huang, D., Wu, Z., and Sunden, B. "Effects of hybrid nanofluid mixture in plate heat exchangers", *Exp. Therm. Fluid Sci.*, **72**, pp. 190–196 (2016).
3. Liu, Y., Wang, Q., Wu, T., et al. "Fluid structure and transport properties of water inside carbon nanotubes", *J. Chem. Phys.*, **123**(23), 234701 (2005).
4. Madhesh, D. and Kalaiselvam, S. "Experimental analysis of hybrid nanofluid as a coolant", *Procedia Eng.*, **97**, pp. 1667–1675 (2014).
5. Toghraie, D., Chaharsoghi, V.A., and Afrand, M. "Measurement of thermal conductivity of ZnO–TiO_2 /EG hybrid nanofluid", *J. Therm. Anal. Calorim.*, **125**(1), pp. 527–535 (2016).
6. Tlili, I., Bhatti, M.M., Hamad, S.M., et al. "Macroscopic modeling for convection of Hybrid nanofluid with magnetic effects", *Phys. A: Stat. Mech. Appl.*, **534**, 122136 (2019).
7. Yang, D., Yasir, M., and Hamid, A. "Thermal transport analysis in stagnation-point flow of Casson nanofluid over a shrinking surface with viscous dissipation", *Waves Random Complex Media*, pp. 1–15 (2021). https://doi.org/10.1080/17455030.2021.1972183
8. Tang, W., Zou, C., Liang, H., et al. "The comparison of interface properties on crude oil-water and rheological behavior of four polymeric nanofluids (nano-SiO_2, nano-CaO, GO and CNT) in carbonates for enhanced oil recovery", *J. Pet. Sci. Eng.*, **214**, 110458 (2022).
9. Upreti, H., Pandey, A.K., and Kumar, M. "Assessment of entropy generation and heat transfer in three-dimensional hybrid nanofluids flow due to convective surface and base fluids", *J. Porous Media*, **24**(3), pp. 35–50 (2021).
10. Hakeem, A.K., Indumathi, N., Ganga, B., et al. "Comparison of disparate solid volume fraction ratio of hybrid nanofluids flow over a permeable flat surface with aligned magnetic field and Marangoni convection", *Sci. Iran.*, **27**(6), pp. 3367–3380 (2020).
11. Upreti, H., Pandey, A.K., and Kumar, M. "Thermophoresis and suction/injection roles on free convective MHD flow of Ag–kerosene oil nanofluid", *J. Comput. Des. Eng.*, **7**(3), pp. 386–396 (2020).
12. Nadeem, S., Amin, A., Abbas, N., et al. "Effects of heat and mass transfer on stagnation point flow of micropolar Maxwell fluid over Riga plate", *Sci. Iran.*, **28**(6), pp. 3753–3766 (2021).

13. Yasir, M., Hafeez, A., and Khan, M. "Thermal conductivity performance in hybrid (SWCNTs-CuO/Ehylene glycol) nanofluid flow: Dual solutions", *Ain Shams Eng. J.*, **13**(5), 101703 (2022).

14. Hafeez, M.B., Khan, M.S., Qureshi, I.H., et al. "Particle rotation effects in Cosserat-Maxwell boundary layer flow with non-Fourier heat transfer using a new novel approach", *Sci. Iran.*, **28**(3), pp. 1223–1235 (2021).

15. Shahid, M.I., Ahmad, S., and Ashraf, M. "Simulation Analysis of Mass and Heat Transfer Attributes in Nanoparticles Flow subject to Darcy-Forchheimer Medium", *Sci. Iran.*, **29**(4), pp. 1828–1837 (2022).

16. Yasir, M., Ahmed, A., and Khan, M. "Carbon nanotubes based fluid flow past a moving thin needle examine through dual solutions: Stability analysis", *J. Energy Storage*, **48**, 103913 (2022).

17. Roberts, L. "On the melting of a semi-infinite body of ice placed in a hot stream of air", *J. Fluid Mech.*, **4**(5), pp. 505–528 (1958).

18. Yacob, N.A., Ishak, A., and Pop, I. "Melting heat transfer in boundary layer stagnation-point flow towards a stretching/shrinking sheet in a micropolar fluid", *Comput. Fluids*, **47**(1), pp. 16–21 (2011).

19. Bachok, N., Ishak, A., and Pop, I. "Melting heat transfer in boundary layer stagnation-point flow towards a stretching/shrinking sheet", *Phys. Lett. A*, **374**(40), pp. 4075–4079 (2010).

20. Hayat, T., Mustafa, M., Shehzad, S.A., et al. "Melting heat transfer in the stagnation-point flow of an Upper-Convected Maxwell (UCM) fluid past a stretching sheet", *Int. J. Numer. Methods Fluids.*, **68**(2), pp. 233–243 (2012).

21. Das, K. "Radiation and melting effects on MHD boundary layer flow over a moving surface", *Ain Shams Eng. J.*, **5**(4), pp. 1207–1214 (2014).

22. Singh, K., Kumar, M., and Pandey, A.K. "Melting and chemical reaction effects in stagnation point flow of micropolar fluid over a stretchable porous medium in the presence of nonuniform heat source/sink", *J. Porous Media,* **23**(8), pp. 767–781 (2020).

23. Singh, K., Pandey, A.K., and Kumar, M. "Numerical solution of micropolar fluid flow via stretchable surface with chemical reaction and melting heat transfer using Keller-Box method", *Propuls. Power Res.*, **10**(2), pp. 194–207 (2021).

24. Hayat, T. and Alsaedi, A. "Development of bioconvection flow of nanomaterial with melting effects", *Chaos Solitons Fractals*, **148**, 111015 (2021).

25. Pop, I., Waini, I., and Ishak, A. "MHD stagnation point flow on a shrinking surface with hybrid nanoparticles and melting phenomenon effects", *Int. J. Numer. Methods Heat Fluid Flow.*, **32**(5), pp. 1728–1741 (2021).

26. Singh, K., Pandey, A.K., and Kumar, M. "Melting heat transfer assessment on magnetic nanofluid flow past a porous stretching cylinder", *J. Egypt. Math. Soc.*, **29**(1), pp. 1–14 (2021).

27. Yasir, M. and Khan, M. "Comparative analysis for radiative flow of Cu–Ag/blood and Cu/blood nanofluid through porous medium", *J. Pet. Sci. Eng.*, **215**, 110650 (2022).

28. Lakshmi Devi, G., Niranjan, H., and Sivasankaran, S. "Effects of chemical reactions, radiation, and activation energy on MHD buoyancy induced nano fluidflow past a vertical surface", *Sci. Iran.*, **29**(1), pp. 90–100 (2022).

29. Swalmeh, M.Z., Alkasasbeh, H.T., Hussanan, A., et al. "Numerical investigation of heat transfer enhancement with Ag-GO water and kerosene oil based micropolar nanofluid over a solid sphere", *J. Adv. Res. Fluid Mech.*, **59**(2), pp. 269–282 (2019).

30. Wang, C.Y. "Stagnation flow towards a shrinking sheet", *Int. J. Non-Linear Mech.*, **43**(5), pp. 377–382 (2008).

Biographies

Kehong Zheng is a Professor at College of Water Conservancy and Ecological Engineering, Nanchang Institute of Technology, Nanchang 330099, China. He is also a member of several editorial boards in well-reputed international journals. Nationally, he is serving on several scientific committees throughout the country.

Syed Irfan Shah is an Associate professor at the Department of Sciences and Humanities, National University of Computer and Emerging Sciences (FAST), A. K. Brohi Road H-11/4 Islamabad, Pakistan. He has published his work in the well-reputed impact-factor international journal.

Muhammad Naveed Khan achieve his MPhil and PhD degrees from the Department of Mathematics at Quaid-i-Azam University, Islamabad, Pakistan. He has published his work in the well-reputed impact-factor international journal.

Elsayed Tag-eldin is working as Assistant Professor at Faculty of Engineering and Technology, Future University in Egypt New Cairo 11835, Egypt. He has published more than 300 research articles in well-reputed international journals having more than 1000 citations.

Muhammad Yasir is a PhD scholar at the Department of Mathematics, Quaid-i-Azam University 45320, Islamabad 44000, Pakistan. He completed his MPhil degree from the Department of Mathematics at Quaid-i-Azam University, Islamabad, Pakistan, and currently is PHD scholar at Department of Mathematics, Quaid-I-Azam University 45320, Islamabad 44000, Pakistan. He has published his work in the well-reputed impact-factor international journal.

Ahmed M. Galal is working as an Assistant Professor at the Production Engineering and Mechanical Design Department, Faculty of Engineering, Mansoura University, P.O 35516, Mansoura, Egypt. He has published more than 200 research articles in well-reputed international journals having more than 600 citations.